Experiments in Fluids 22 (1996) 137–143 © Springer-Verlag 1996

Adoption of a genetic algorithm (GA) for tomographic reconstruction of line-of-sight optical images

K. D. Kihm, K. Okamoto, D. Tsuru, H. S. Ko

Abstract A new tomographic reconstruction scheme is proposed that uses a genetic algorithm (GA), a robust and combinatorial function optimization based on the mechanics of the genetic principle. The paper first discusses the implicitly parallel and scaled random nature of the GA optimization using an illustrative example. An introduction of the elementary distribution function (EDF) to constitute the cross-sectional field shows a successful adoption of GA for optical tomography. The GA-based tomography was examined for interferometric projections of computer-synthesized phantom density fields. The GA-based tomography shows accurate and stable image reconstruction, particularly for limited projections.

List of symbols

A_i	magnification factor of the ith EDF
ART	algebraic reconstruction technique
CT	computer tomography
D	diameter of an axisymmetric test field or diffusion coefficient (Eq. (2a))
EDF	elementary distribution function
f	type of elementary distribution function
F	fitness value (Eq. (4))
FC	Fourier convolutions
GA	genetic algorithm
I	number of individuals in population
K	Gladstone-Dale constant (0.226×10^{-3} m^3/kg at $\lambda = 632.8$ nm for air at 288 K and 101.3 kPa)
MRI	magnetic resonance imaging
n	index of refraction or the number of EDFs
n_o	index of refraction in vacuum
N	fringe shift number
N_R	number of children created in each generation
p	measured projection
p^*	virtual projection
PIV	particle image velocimetry
r	radial coordinate of axisymmetric test field
R	coordinate perpendicular to the line-of-sight direction (Fig. 6)
RMS	root mean square
S	coordinate parallel to the line-of-sight direction (Fig. 6)
t_i	shape factor of the ith EDF
t	time
x, y	rectangular coordinate system defined on the test field (Fig. 6)
δ	Dirac-delta function
θ	projection angle
λ	laser wave length (632.8 nm for helium-neon laser)
ρ	gas density

Received: *6 November 1995 / Accepted*: *6 May 1996*

K. D. Kihm, H. S. Ko
Department of Mechanical Engineering, Texas A&M University
College Station, TX 77843-3123, USA

K. Okamoto, D. Tsuru
Nuclear Engineering Research Laboratory, University of Tokyo
Tokai-mura, Ibaraki 319-11, Japan

Correspondence to: K. D. Kihm

1 Introduction

Most optical visualization techniques measure line-of-sight projected images that integrate optical information along the beam path occupied by a test field. Unless the optical information is uniformly distributed along the beam path, a sophisticated reconstruction process is necessary to recover the cross-sectional field information from the projected images. Such procedures are generally called optical tomography or tomographic image reconstruction.

An axisymmetric test field requires only a single projection at any arbitrary projection angle to reconstruct the cross-sectional information that varies only along the radius (Deans 1983). For asymmetric test fields, however, a number of projections from many different angles must be simultaneously interrogated to optimally determine the cross-sectional information. Stacking up the reconstructed two-dimensional information will construct a full three-dimensional field. Exist ing tomographic techniques belong to either of two primary categories: a direct mathematical inversion calculation of the cross-sectional field from projected images (Kak and Slaney 1987; Liu et al. 1989) or a successive iteration of the field by regression optimization (Sweeney and Vest 1973, Rangayyan et al. 1985).

The former category, referred to as Fourier convolutions (FC) based on the Fourier slicing theorem (Brigham 1988), usually requires a large number of equally angled projections to ensure its mathematical stability and acceptable accuracy. The requirement of multiple projections is achieved by either scanning a detector around a test object when the test field

remains unchanged during the scanning time, or by installing as many detectors as needed around the test field for simultaneous imaging of a time-dependent field (Hesselink 1989). Spatial and other constraints often limit the number and interval of projections. Thus, the reconstruction accuracy of the FC technique can be degraded for the case of limited projections (Goulard and Emmerman 1980). The FC technique is widely used for medical imaging systems such as MRI (magnetic resonance imaging) or CT (computer tomography), where the field (patient's body) remains steady during the period of multiple image detections and allows hundreds of equally angled images. However, other problems involving time-dependent phenomena will make a simultaneous recording necessary.

The latter category of regression optimization, represented by the algebraic reconstruction technique (ART), needs fewer projections for a stable reconstruction and the projections do not need to be equally angled (Gordon 1974). However, since the ART is a monotonic optimization searching for the gradient, it lacks true robustness and inherently carries a danger of entrapment by a local peak (Swindell and Barrett 1977). Also, when the number of iterations exceeds a certain optimum the ART can increase artifacts and destroy the reconstruction (Decker 1993). In addition, the iterative reconstruction procedure requires the feedback information obtained from comparing the measured projection of the actual field with the virtual projection from the guessed field. The discrepancy between the two fields is back projected to update the previously guessed field and the iterative cycle repeats until a convergence is met.

When the forward projection is a linear summation of the field values along the light ray, the back projection of the feedback information is easily obtained. Fortunately, many optical projections devise a linear summation of the field. For example, all images based on light attenuation, such as X-ray imaging in proportion to the medium density, MRI based on the isotope concentration, and interferometry where the fringe counting is directly dependent on the field density. However, for nonlinear imaging such as laser speckle photography (Merzkirch 1987), the back projection of the feedback signal is not readily obtained and the ART regression will not proceed efficiently. Nevertheless, the simple and straight features of ART techniques are widely accepted for linear projection problems (Verhoeven 1993).

The Genetic Algorithm (GA) is a robust, intelligent, and combinatorial function optimization algorithm for finding unknowns (cross-sectional information) from a set of knowns (measured projected images) based on the mechanics of the genetic principle. The genetic principle implies natural selection and survival of the fittest based on parallelism, elitism, and scaled randomness (Goldberg 1989). Computer scientists and mathematicians have recognized the superiority of GA in finding solutions over other optimization schemes. The key idea of this paper is that the combinatorial and robust features of GA can contribute to establishing a new tomographic method to alleviate the aforementioned problems associated with existing techniques. The robust feature of GA is expected to overcome the local-peak-locking problem with progressive optimization. The regression feature of GA can achieve a stable reconstruction without an excessive number of projections.

Literature on engineering applications of GA is scarce. Tsukiji et al. (1994) proposed a new GA particle tracking method to improve the effectiveness in identifying particle pairs between sequential flow images for PIV (particle image velocimetry). They showed that GA was advantageous in that the particle image pairs were identified faster and more accurately compared with the conventional correlation method. The pioneering work by Tsuru et al. (1994) is the first and only published attempt to use GA for tomographic flow visualization. Their results showed a viability of the GA-based tomography. This paper describes the principle of GA and its application for tomography. Some example applications of the newly developed GA-based tomography will demonstrate its potential in accurate image reconstruction, particularly under limited projections.

2
Genetic algorithm (GA)-based tomography

Section 2.1 uses an illustrative example to introduces the essential features of the genetic algorithm (GA). Section 2.2 explains the idea to use the Elementary Distribution Function (EDF) as a basis function. The optimization procedure of the GA-based tomography is summarized for an arbitrary and asymmetric density field in Sect. 2.3. Section 2.4 presents a mathematical expression for interferometric projection to be used as an example projection function for this study.

2.1
What is GA in view of optical tomography

The unique feature of GA and its adoption for optical tomography are illustrated in Fig. 1, using an axisymmetric density field under interferometric imaging. An axisymmetric density field is reconstructed from a single line-of-sight interferometric image at any arbitrary projection angle. Determining the unknown density values at all the nodal points can be optimized with GA, a search procedure based on the mechanics of natural selection and natural genetics (Holland 1975). Although the goal is to find one optimized set of $(\rho_1, \rho_2, \ldots, \rho_{10})$, the GA initiates and proceeds with a population of I individuals or solution candidates. Each individual carries randomly assigned initial guesses for the field $(\rho_1^i, \rho_2^i, \ldots, \rho_{10}^i)$ for $i = 1, 2, \ldots, I$. This feature of handling multiple individuals is called "implicit parallelism." The density values at the discrete nodal points, $\rho_1^i, \rho_2^i, \ldots, \rho_{10}^i$, are treated as "genes" of the ith individual. Successive generations

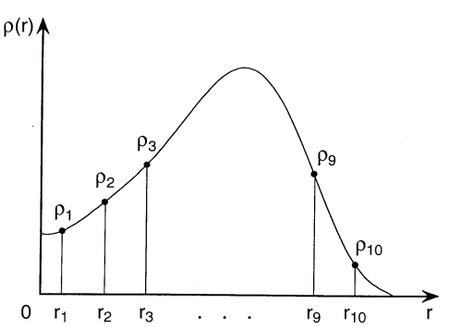

Fig. 1. An axisymmetric density distribution with discrete unknowns

evolve following the genetic principle of the natural selection and fittest survival with a scaled random principle.

The degree of deviation of each individual's projection from the measured projection of the actual field is "fitness" of the individual with a higher fitness referring to a smaller deviation. In proportion to the fitness, each individual is assigned a "mating probability." Individuals with higher mating probabilities form a "mating pool." Instead of assigning the mating probability, the number of mating couples can be specified for a straightforward GA operation. A scaled random selection allows two individuals to swap their genes or "crossover" for two new children. Then only two individuals out of the four (two parents and two children) with the highest fitness values survive the generation.

Genes within an individual carry a specified mutation probability and genes are subjected to mutate randomly to create a mutant individual. Again, the number of mutations can be specified. Only the individual with the higher fitness survives among the original and the mutant. The primary role of the mutation of genes is to prevent individuals from settling at a local peak, and to provide a robust feature in searching for the ultimate peak. Any twin or triplet individuals will count as one to avoid the potential of "dominance by common." A new generation evolves from the set of procedures of selection, crossover, mutation, and fitness evaluation up to a given number of generations or until the first ranked individual with the highest fitness falls within a specified tolerance. The genes carried by this individual determine the optimized density field.

2.2
Elementary distribution function (EDF)

To enhance the spatial resolution of the reconstructed field without significantly increasing the computational expense, the discrete density value at each nodal point r_i is replaced by an elementary distribution function $f(r-r_i;\ A_i,\ t_i)$ where A_i and t_i represent its magnification and shape factor, respectively (Fig. 2). The density field is assumed to conform to the summation of all the elementary distribution functions, i.e.,

$$\rho(r) = A_i \sum_{i=1}^{10} f(r-r_i;\ t_i) \tag{1}$$

The reconstruction problem now reduces to find an individual carrying optimized "genes" of $(A_1, t_1, A_2, t_2, \ldots, A_{10}, t_{10})$. This solution finding is performed by manipulating the

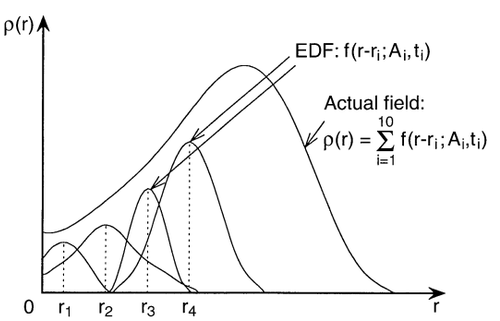

Fig. 2. Correspondence between the density distribution and superposed elementary distribution functions (EDF)

above-discussed genetic algorithm procedures of selection, crossover, mutation, and fitness evaluation.

Though the number of unknowns has apparently increased by a factor of two in the example (twenty from ten), when the discretely set density values are replaced by elementary distribution functions (EDFs), the spatially resolved accuracy has improved to that of the continuous elementary distribution function. Also, since each EDF extends over the entire field, the number of EDFs necessary to describe the field is expected to be fewer than the number of nodal points required for discrete unknowns. This implies that the GA-based tomography associated with EDF can perform the image reconstruction from a smaller number of unknowns (projected data) than with discrete unknowns.

In principle, EDF can be any type of continuous function such as Gaussian, Rayleigh, sine or cosine, mass diffusion, or log-normal. Proper discretion in selecting a function for EDF to best represent the physical conditions of a tested field may expedite the reconstruction optimization. For example, an air jet diffused into a helium environment may select a mass diffusion solution for EDF, since the diffusion equation describes the physical nature of the jet. A normalized mass concentration profile $f(r, t)$ for a radial mass diffusion process is obtained by solving the diffusion equation in the cylindrical coordinate system,

$$\frac{\partial f(r,t)}{\partial t} = D\frac{1}{r}\frac{\partial}{\partial r}\left(r\frac{\partial f}{\partial r}\right) \tag{2a}$$

where the initial and boundary conditions are given as

$$f(r,0) = 1 \quad (r \leqslant r_{\text{source}}) \tag{2b}$$

$$0 \quad (\text{otherwise}) \tag{2c}$$

$$f(\infty, t) = 0 \tag{2d}$$

and the flow field is assumed to consist of multiple sources of radius r_{source}, equal to one-half the distance between the calculation nodes. D is the diffusion coefficient and can be given an arbitrary value. The EDF $f(r, t)$ calculated from Eq. (2a) together with conditions of Eqs. (2b–d) is shown in Fig. 3. A linear combination of these EDFs of mass diffusion type now conforms to the computer synthesized phantom fields tested in this study.

2.3
Calculation procedure of the GA-based tomography

For an arbitrarily two-dimensional test field (Fig. 4), the density distribution, which is asymmetric, is expressed as an extended form of Eq. (1):

$$\rho(x,y) = \sum_{i=1}^{n} A_i f(\sqrt{(x-x_i)^2+(y-y_i)^2};\ t_i) \tag{3}$$

where (x_i, y_i) represents the location of the ith nodal point corresponding to the center of EDF. The density distribution $\rho(x, y)$ can be obtained by determining an optimized set of the magnification and shape factors, $(A_1, t_1, A_2, t_2, \ldots, A_n, t_n)$ where n denotes the total number of EDFs considered for the entire test field.

The GA-based tomography treats the n-sets of magnification and shape factors as genetic genes or "chromosomes" carried

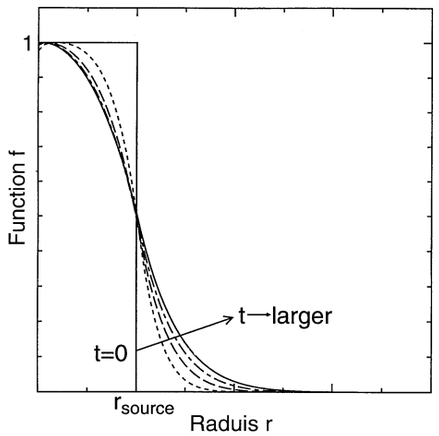

Fig. 3. Normalized mass diffusion function for different shape factors

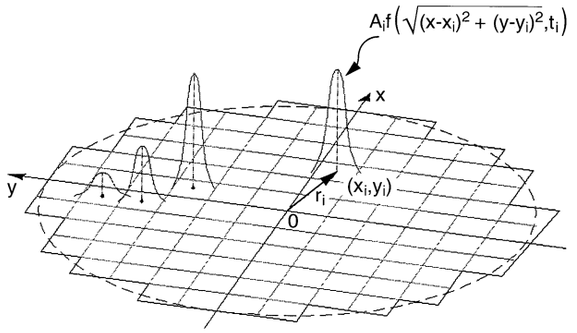

Fig. 4. Schematic illustration of a density distribution composed of a summation of elementary distribution functions (EDFs)

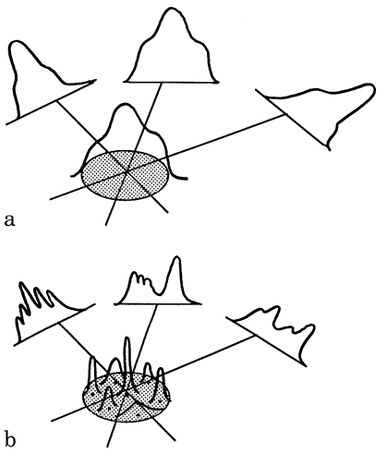

Fig. 5a, b. Measured projections and virtual projections

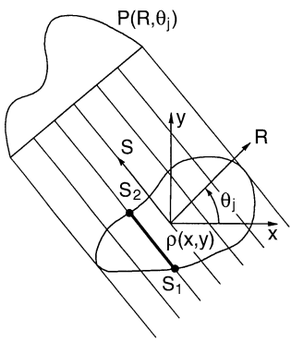

Fig. 6. Cross-sectional and projected plane coordinate systems

by an individual. An initial population group $I=100$, for example, may be created and each individual in the group carries randomly assigned initial values of (A_1, t_1, A_2, t_2, … , A_n, t_n). Each of the initially assigned individuals constructs a density distribution from Eq. (3) and this density distribution generates projected images at different imaging angles. These images projected from each solution candidate are called *virtual projections* and the actual projections of the density field are called *measured projections* (Fig. 5).

Fitness value F of one individual is defined as the normalized RMS deviation of the virtual projections from the measured projections, i.e.,

$$F=\frac{\sqrt{\sum_j \int_{-\infty}^{\infty} |p(R,\theta_j)-p^*(R,\theta_j)|^2\,\mathrm{d}R}}{\sum_j \int_{-\infty}^{\infty} |p(R,\theta_j)|\,\mathrm{d}R} \tag{4}$$

where p and p^* denote measured and virtual projections, respectively, R represents the horizontal coordinate on the projection plane at θ_j projection angle (Fig. 6), and j is the number of projections at different projection angles. A highly fitted individual carries a small fitness value F, and a less fitted individual carries a larger fitness value. In every generation, the better individuals are copied to the following generation and the worst individuals are removed. Note that the only feedback information required to continue the solution searching in GA is the fitness values. The optimization is carried out within the solution candidates by themselves with no need of back projection. Therefore, the GA-based tomography can alleviate the difficulty associated with the feedback projection in ART for nonlinear projection problems.

Each generation consists of *Selection*, *Crossover for Reproduction*, *Mutation*, *and Ranking*. Two individuals are selected from a tier of high rankers based on the scaled random principle discussed in the previous section. This selected couple reproduces two children by crossover of their genes under a controllably random manner. The number of reproductions N_R can be arbitrarily specified, for example, $N_R=20$, or a certain reproduction probability can be assigned to each individual without specifying N_R.

Some randomly selected individuals are mutated to replace all or part of their genes. This prevents individuals from settling at local minimum of fitness values and to provide more robust optimization in searching for the ultimate peak. All individuals are ranked by their fitness values and individuals ranked beyond I are eliminated from the group so that the next generation starts with no population increase. A new generation evolves by the set of procedures of *Selection*, *Reproduction*, *Mutation*, and *Ranking*, and the evolution continues until the fitness value (Eq. (4)) of the first ranked individual falls within a specified tolerance. The genes, or the equivalent optimized magnification and shape factors, carried by this individual determine the density distribution of Eq. (3).

In summary, the GA-based tomographic image reconstruction is an innovative regression method using a robust and multi-dimensional optimization based on the scaled random principle. The stochastic and scaled-random GA regression method does not need feedback information by back projection of the projected images, while existing ART methods rely on the back projection of projected images, for successive iterations of the reconstructed field. The natural selection mechanics of the genetic principle automatically and statistically upgrade the solution field.

2.4
Interferometric projection of density field

Fermat's principle (Born and Wolf 1959) states that the wavelength of light becomes shorter in a medium with refractive index n compared with the wave length in vacuum ($n_o = 1.0$). When light rays travel through the test section with refractive index distribution $n(x, y)$ in the projection direction S (Fig. 6), the number of waves increases within the test section compared with that for a vacuum, $N(R)$, and is expressed as

$$N(R) = \frac{1}{\lambda} \int_{S_1}^{S_2} [n(x, y) - n_0] \, \mathrm{d}S \tag{5}$$

For finite-fringe interferometry, $N(R)$ is identical to the number of crossing fringes recorded on the projected images. The refractive index can be converted to the medium density using the Gladstone-Dale relationship (Vest 1979)

$$n(x, y) = 1 + K \cdot \rho(x, y) \tag{6}$$

where the Gladstone–Dale constant K is a function of wavelength. Combining Eqs. (5) and (6), the interferometric projection function is derived. For example, an air jet into a helium environment:

$$p(R, \theta_j) = N(R) = \frac{K(\rho_{\mathrm{Air}} - \rho_{\mathrm{He}})}{\lambda} \int_{S_1}^{S_2} \left[\frac{\rho(x, y) - \rho_{\mathrm{He}}}{\rho_{\mathrm{Air}} - \rho_{\mathrm{He}}} \right] \mathrm{d}S. \tag{7}$$

Similarly, when $S_1 = S_1(x_1, y_1)$ and $S_2 = S_2(x_2, y_2)$,

$$p(R, \theta_j) = \frac{K}{\lambda} \int_{y_1}^{y_2} \int_{x_1}^{x_2} g(x, y) \delta(x \cos\theta_j + y \sin\theta_j - R) \, \mathrm{d}x \, \mathrm{d}y \tag{8}$$

where the density distribution $g(x, y) \equiv \rho(x, y) - \rho_{\mathrm{He}}$ can also be expressed in terms of EDFs by Eq. (3). δ represents a Dirac-delta function that is equal to 1 for $x \cos\theta_j + y \sin\theta_j - R = 0$, and 0 otherwise.

For an axisymmetric test field, which requires only a single projection, Eq. (7) reduces to the Abel type integration (Deans 1983) as

$$p(y, \theta = \theta_{\mathrm{arbitrary}}) = N(y) = \frac{2K(\rho_{\mathrm{Air}} - \rho_{\mathrm{He}})}{\lambda} \int_{y}^{D/2} \left[\frac{\rho(r) - \rho_{\mathrm{He}}}{\rho_{\mathrm{Air}} - \rho_{\mathrm{He}}} \right] \frac{r \, \mathrm{d}r}{\sqrt{r^2 - y^2}}. \tag{9}$$

where D is the diameter of the axisymmetric test field. For an axisymmetric test field, no distinction is needed between the x–y and S–R coordinate systems since no relative rotation of the projection is necessary.

3
Results and discussion

The computer program for the GA-tomographic reconstruction calculations has been coded with the C and C^{++} languages. A computer synthesized phantom density field simulates the present example of an air jet into a helium environment. The projection data of the fringe shift numbers were calculated from the reference phantom field using the interferometric projection function in Eqs. (7) or (8). The GA-based tomography reconstructed the cross-sectional density field from these (pseudo) measured projections and the reconstructed field was examined against the reference field.

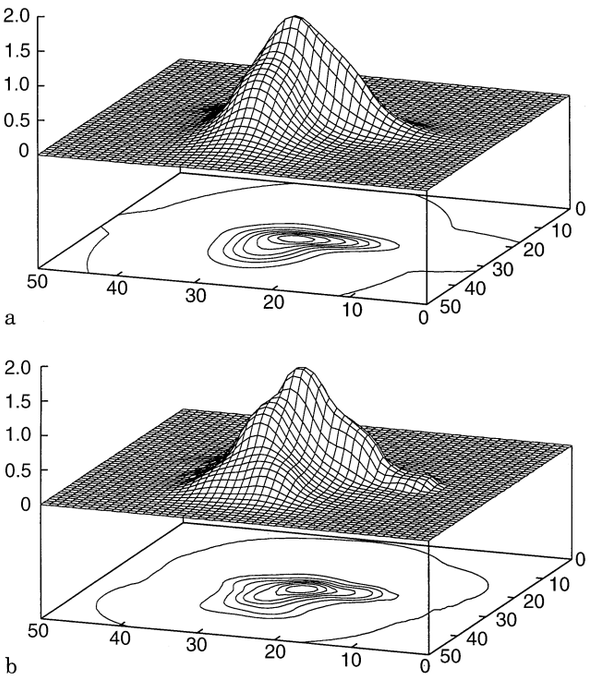

Fig. 7a, b. Asymmetric distorted density field **a** computer synthesized reference density distribution; **b** reconstructed density distribution after 1,000 generation of the Genetic Algorithm (GA)-based tomography with six equally-angled interferometric projections

The viability of the GA-based tomographic scheme has been examined using an asymmetric single peak reference field (Fig. 7a). The peak location is skewed from the center of the test field and the peak density extends above 1.4 in an arbitrary unit. The computation was carried out on a Pentium 90 MHz PC machine at the University of Tokyo. The number of GA generations was expanded to 1000. The mass diffusion solutions were selected for the EDF type and a total of 19 computational nodal points were set for 19 EDFs. Interferometric projections were considered at six equal angular intervals, $\theta = 0^\circ$, 30°, 60°, 90°, 120°, and 150°. The GA conversion used a population of 100 individuals with 20 children born in each generation.

The GA-based conversion (Fig. 7b) successfully identifies the locations and shapes of the ridges, accurately predicts the peak density height of approximately 1.4, and shows close proximity in the density contour map with its counterpart of the reference field. The high accuracy of the reconstructed results shows the effectiveness of the GA-based tomography.

The band of symbols in Fig. 8 shows the evolving history of the fitness values (Eq. (4)) for the population of 100 individuals. Fitness values quickly decreased during the beginning

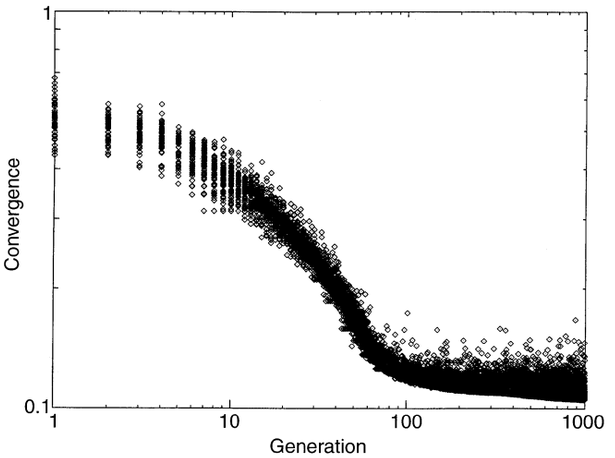

Fig. 8. Convergence values of the whole population of 100 individuals versus the generation evolution for the GA-based reconstruction shown in Fig. 7b

100 generations or so, and gradually approached the minimal level. The best (or smallest) fitness value decreased consistently with evolving generations, while the range of fitness values in each generation scatters. This means that the worst or largest fitness value does not necessarily improve with generations while the top individual consistently improves. This explains the "elitism" imposed in the GA optimization, which focuses on improving the elite members rather than remedying the bad individuals, since it is the best individual that leads the optimization. Along the same strategy, the best individual of the current generation replaces the best individual of the previous generation but only if the former outperforms the latter. In other words, the best individual keeps its title until a new challenger wins the title.

Figure 9a shows the second phantom composed of 90 identical EDFs of the mass diffusion solution type and one taller EDF of the same type. The GA-based tomography started with 91 randomly created EDFs of the same mass diffusion type but with randomly assigned A_i's and t_i's. The reconstruction was carried out from six interferograms mathematically projected at six different angles with equal intervals. Each generation held a population of 40 with 20 children and up to 20 allowable mutations. The calculations were carried out on the CRAY-YMP super computer platform available at Texas A&M University. Figure 9b shows the reconstructed field by the top individual of the 1000 th generation. The GA-based tomography precisely reconstructs the shape and location of the peak and fairly well determines the isochoric contours.

For more critical testing, the GA-based tomography is applied to reconstruct an asymmetric reference density field consisting of two singular peaks (Fig. 10a). The GA operating parameters, such as the number of individuals, the number and type of EDFs, the number of children, the number of mutation, and the number of generations, remained the same as in Fig. 9. The reconstruction result (Fig. 10b) shows a fairly acceptable distribution identifying the locations of the two peaks. However, the GA method was unable to reconstruct the exact shape of these singular peaks. The contour map of the results also shows fairly good agreement with the contour map of the

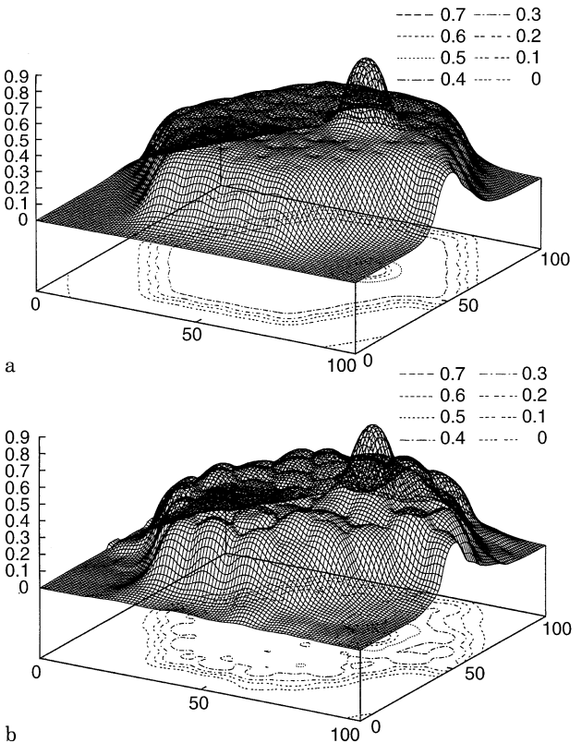

Fig. 9a, b. Density field with a skewed peak **a** computer synthesized reference distribution; **b** reconstructed density distribution after 1000 generations of the genetic algorithm (GA)-based tomography with six equally-angled interferometric projections

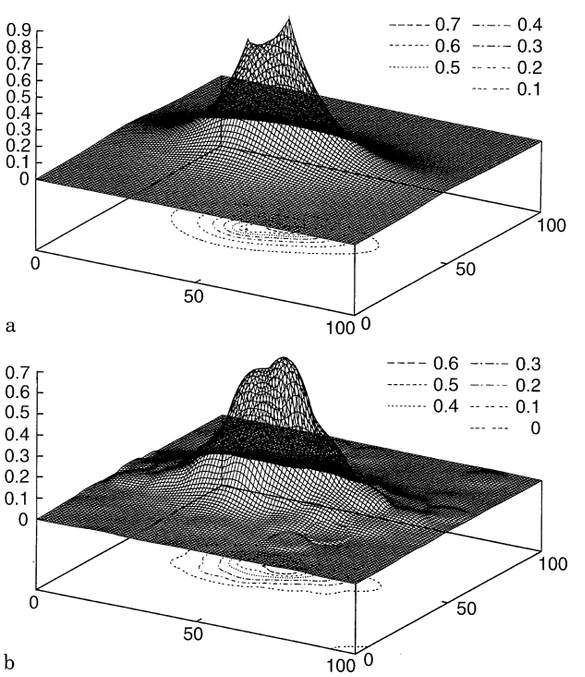

Fig. 10a, b. Singular twin-peak density fields **a** computer synthesized reference distribution; **b** reconstructed density distribution after 1000 generations of the genetic algorithm (GA)-based tomography with six equally-angled interferometric projections

reference field. The discrepancies between the reference and reconstructed shapes is mainly because of the excessive differences between the singular peaks of cusp and bell shape EDFs of the mass diffusion solution type. It is expected that a more elaborate selection of EDFs could significantly improve the reconstruction accuracy of such a singular field.

4 Concluding remarks

A new tomographic reconstruction scheme using GA has been successfully developed and applied to computer generated phantom fields to examine its potential as a better means for optical image reconstruction. The GA-based tomography reconstructs the cross-sectional field with fairly good accuracy, particularly for the limited projections of six. The GA method requires a longer computer CPU time than other conventional regression techniques because of its highly combinatorial optimization feature. It will be worthwhile to extensively examine the effects of the genetic operators, such as the number and type of EDFs, the ratios of crossovers and mutations upon the reconstruction accuracy. A rigorous comparison will require a systematic examination of the performance of the GA-based tomography against other existing tomographic methods based on both mathematical inversions and iterative regressions.

References

Born M; Wolf E (1959) Principle of Optics. Pergamon Press, Oxford: 128–130

Brigham EO (1988) The fast Fourier transform and its applications. Prentice-Hall, Englewood Cliffs, NJ

Deans AR (1983) The Radon transform and some of its applications. Wiley, New York

Decker AJ (1993) Tomographic methods in flow diagnostics, NASA Report No. 106330

Goldberg DE (1989) Genetic algorithms in search, optimization & machine language. Addison-Wesley, Reading

Gordon R (1974) A tutorial on ART. IEEE Trans. NS-21: 78–92

Goulard R; Emmerman PJ (1980) Combustion diagnostics by multiangular absorption. In: Inverse scattering problems in optics. Springer, Berlin

Hesselink L (1989) Optical tomography. In: Handbook of flow visualization (Yang, W-J ed.): Hemisphere, New York: Ch. 20

Holland JH (1975) Adaptation in natural and artificial systems. MIT Press, Cambridge

Kak AC; Slaney M (1987) Principles of computerized tomographic imaging. IEEE Press, New York.

Liu TC; Merzkirch W; Oberste-Lehn K (1989) Optical tomography applied to speckle photographic measurement of asymmetric flows with variable density. Exp Fluids 7: 157–163

Merzkirch W (1987) Flow visualization. Academic Press, Orlando, Ch. 3

Rangayyan R; Dhawan AP; Gordon R (1985) Algorithms for limited-view computed tomography: an annotated bibliography and a challenge. Appl Opt 24: 4000–4012

Sweeney DW; Vest CM (1973) Reconstruction of three-dimensional refractive index fields from multidirectional interferometric data. Appl Opt 12: 2649–2664

Swindell W; Barrett HH (1977) Computerized tomography: taking sectional X rays. Phys Today, December: 32–41

Tsukiji T; Ohyama R; Kaneko K (1994) Investigation of particle tracking method using genetic algorithm. Proc. 3rd Asian Symposium on Visualization, Chiba, Japan 663–668

Tsuru D; Okamoto K; Madarame H; Fumizawa M (1994) Measurement of density distribution using optical tomography with genetic algorithm. Proc. 4th Fluid Control, Measurement and Visualization (FLUCOME 94), Toulouse, France: 971–976

Verhoeven D (1993) Limited-data computed tomography algorithms for the physical sciences. Appl Opt 32: 3736–3754

Vest CM (1979) Holographic interferometry. J Wiley, New York, 344–377